Journal of Alloys and Compounds 708 (2017) 422–427

Contents lists available at ScienceDirect

Journal of Alloys and Compounds

journal homepage: http://www.elsevier.com/locate/jalcom

Nanoprecipitation effects on phase stability of Fe-Mn-Al-Ni alloys

P. La Roca [a, b], A. Baruj [a, b], C.E. Sobrero [c], J.A. Malarría [c], M. Sade [a, b, *]

[a] Centro Atómico Bariloche (CNEA), Instituto Balseiro (U.N. Cuyo – CNEA), Av. Bustillo 9500, 8400, S.C. de Bariloche, Río Negro, Argentina
[b] Consejo Nacional de Investigaciones Científicas y Técnicas (CONICET), Argentina
[c] Instituto de Física Rosario – CONICET-UNR, Rosario, Argentina

ARTICLE INFO

Article history:
Received 25 October 2016
Received in revised form
21 February 2017
Accepted 27 February 2017
Available online 28 February 2017

Keywords:
Pseudoelasticity
FeMnAlNi alloys
Precipitation
Martensitic transformation

ABSTRACT

Early stages of coherent precipitation have been studied in several Fe-Mn-Al-Ni samples aged at 200 °C for different time intervals in order to analyze the effect of nanoprecipitation on the phase stability during thermally induced martensitic transformations. The α-γ′ martensitic transformation was studied by means of dilatometry measurements. Transmission electron microscopy (TEM) observations were performed in order to characterize the microstructure of the samples. The size and volume fraction of nanoprecipitates were evaluated for the as-quenched material and samples aged for 10, 20 and 180 min. Considering these data and additional high resolution TEM results reported in the literature a phenomenological model is presented that enables understanding the effects of B2 precipitates on the relative phase stability between austenite and martensite, and their influence on the observed pseudoelasticity of this metallic system. With this model, the changes of the measured transformation temperatures can be predicted with considerable accuracy.

1. Introduction

Pseudoelasticity is a characteristic property of several shape memory alloys (SMAs) [1]. The potential applications of this property granted a sustained interest for its study. The pseudoelastic behavior of SMAs is related to a thermoelastic martensitic transformation between a high temperature (austenite) phase and a low temperature (martensite) phase. Pseudoelasticity has been widely studied in two alloy systems, i.e. Cu-based and Ni-Ti alloys. Cu-based systems show extremely good properties particularly when single crystals are considered. However polycrystalline alloys show reversibility problems and/or brittleness. Ni-Ti polycrystalline alloys are considered as very good candidates for technological applications, mainly due to their biocompatibility [2]. However this material cannot be cold rolled to obtain deformations larger than 30%, and is considerably expensive for technological devices.

During the last 5 years new pseudoelastic systems have been found. Two Fe-based systems, i.e., Fe-Ni-Co-Al-Ta and Fe-Mn-Al-Ni have been developed and attracted much attention due to their excellent pseudoelastic properties, lower relative cost and better deformability [3–6]. Research on pseudoelastic systems has strongly increased due to these new systems and their potential applications.

Concerning the development of Fe-Mn-Al-Ni pseudoelastic alloys, a significant result was reported by Ando et al. [7]. They analyzed the ternary alloy $Fe_{49}Mn_{36}Al_{15}$ (at.%) finding that an unusual non-thermoelastic martensitic transformation takes place in this system between a disordered high temperature bcc austenite (α) and a fcc martensite (γ′). The subsequent addition of Ni to the alloy system gives place to the precipitation of an ordered bcc structure (B2 order) in the matrix after ageing at 200 °C. The presence of these ordered and coherent precipitates is related to a change in the character of the martensitic transition, which becomes thermoelastic. This phenomenon has been observed in the $Fe_{43.5}Mn_{34}Al_{15}Ni_{7.5}$ (at.%) alloy containing Ni-rich nanoprecipitates, where martensitic variants form under applied stress and disappear in a reversible way [4]. The related pseudoelastic effect allows the reversible recovery of deformations up to 6% at room temperature. In addition, the thermally induced martensitic transformation temperature (M_s) is strongly affected by the presence of precipitates [4].

In fact, Fe-Mn-Al-Ni and Fe-Ni-Co-based alloys show several features in common. In all cases, nanometric precipitates coherent with the austenite play a significant role on the thermoelastic

* Corresponding author. Centro Atómico Bariloche (CNEA), Instituto Balseiro (U.N. Cuyo – CNEA), Av. Bustillo 9500, 8400, S.C. de Bariloche, Río Negro, Argentina
E-mail address: sade@cab.cnea.gov.ar (M. Sade).

http://dx.doi.org/10.1016/j.jallcom.2017.02.280
0925-8388/

character of the transformation. Additionally, precipitation causes a strong shift of the M_s temperatures and increases the pseudoelastic window, i.e., the temperature range where the pseudoelastic behavior occurs. However, it should be taken into account that evolution of precipitates is linked to a change in chemical composition and a change of transformable volume fraction [8]. It is currently accepted that the main role of precipitates in the Fe-Ni-Co system is to harden the involved structures, decreasing microplasticity which, in turn, increases the reversibility of the martensitic transformation [3,9,10,11].

Fe-Mn-Al-Ni pseudoelastic alloys show two additional interesting properties: a) the critical stress to induce the martensite has a weak temperature dependence (around 0.53 Mpa/°C according to Ref. [4]), thus increasing the effective pseudoelastic effect temperature range; b) there is a strong difference in magnetic properties between austenite and martensite, which enables using magnetization measurements for sensing reversible deformations [12].

It is noticed that good superelastic properties are found in Fe-Mn-Al-Ni alloys if bamboo microstructure is used, i.e., the grain size is larger than cross-section of the sample [4,5,13]. Recently, Omori et al. have shown that this type of microstructure is obtained after thermal cycling between 1200 °C and temperatures in the range 600 up 1000 °C, i.e. cycling between temperatures where the bcc and fcc phases are stable [14].

In the last few years, two research groups have published results concerning two significant aspects: on one hand research performed on single crystalline materials increased the understanding on the effect of nanoprecipitates on the pseudoelastic effect [8,15–16]. On the other hand, considerable effort was devoted to the development of polycrystalline materials showing a large reversible deformation. Improvements in this area have been obtained by applying different processing methods and thermal treatments [13,16–19]. Tseng et al. compared the compressive and tensile behaviors of $Fe_{43.5}Mn_{34}Al_{15}Ni_{7.5}$ single crystalline samples oriented parallel to $[100]_{bcc}$. They found that the samples stressed in compression transformed into two martensite variants, obtaining in this way a larger reversibility if compared with the tensile stressed samples where a single martensite variant was induced [15]. These authors also analyzed the evolution of precipitation after thermal ageing at 200 °C, indicating that after 3 h the distribution and size of B2 precipitates optimize the pseudoelastic cycle leading to a large reversibility [8]. Recently, Vollmer et al. reported that, in a polycrystalline sample of $Fe_{43.5}Mn_{34}Al_{15}Ni_{7.5}$, small cracks developed in the grain boundaries of the α phase after quenching. The formation of cracks could be prevented by decreasing the cooling rate due to the formation of γ phase zones in grain boundaries [17].

As it was already mentioned, the microstructure plays a significant role in the generation of pseudoelasticity in Fe-Mn-Al-Ni alloys [8,13]. In fact, it is necessary to introduce Ni-rich precipitates in order to obtain the pseudoelastic behavior in this system. The presence of precipitates appears to distort the stress induced martensite [20]. However, this issue has not yet been completely clarified. One of the goals of the present manuscript is to address this point.

The reported effect of the presence of nanoprecipitates on the M_s temperatures indicates that precipitation strongly alters the relative stability of the involved phases as we previously mentioned in Ref. [21]. Another goal of this manuscript is to add to the understanding of the effect of precipitation on the thermally induced martensitic transition in the Fe-Mn-Al-Ni system. The first stages associated to the formation of precipitates are considered and a phenomenological model taking into account their influence on the martensitic transition is presented.

2. Experimental procedure

A button weighting 15 g of the $Fe_{43.5}Mn_{34}Al_{15}Ni_{7.5}$ alloy was arc melted under Ar atmosphere. The material was thermally treated at 1000 °C for 48 h enclosed in a quartz tube under Ar atmosphere in order to homogenize the alloy composition. Afterwards, it was water quenched by breaking up the capsule. The alloy was then hot rolled at 1000 °C decreasing its thickness down to 1.5 mm (≈80% reduction). Dilatometry samples (10 × 3 × 3 mm^3) were cut, thermally treated for 30 min at 1200 °C and water quenched at room temperature in order to retain the bcc structure (α) in a metastable state. Quenching was performed as fast as possible, leading to a negligible amount of gamma phase at the grain boundaries [17]. The obtained grain sizes ranged from 500 to 900 μm. These samples were subjected to further ageing treatments at 200 °C for different time intervals. Dilatometry measurements were performed on the samples down to liquid nitrogen temperature. A home-made dilatometer was used where a Hottinger WIE linear variable differential transformer (LVDT) is connected to the sample via a quartz tube. A thermocouple welded on the surface of the samples was used to measure the temperature during the measurements. Samples designation and the corresponding thermal treatments are presented in Table 1. Thin foils for TEM analysis were prepared by mechanical grinding and subsequent double jet electropolishing in a solution of 5:95 perchloric acid in acetic acid at 10 °C and 40 V of applied voltage. A Philips CM200 electron microscope was used to observe the microstructure and to measure the density and size of precipitates after the different thermal treatments. In order to determine the size distribution of precipitates, a large amount of dark field images was used for each simple. The diameter of the precipitates was precisely measured for each image. This allowed to perform a statistical analysis. In fact, in a previous report, curves showing the size distribution for the as-cast condition and for samples after 3 h of thermal ageing at 200 °C were reported [21]. The same procedure was used for samples T10 and T20. In this way the average size of the nanoprecipitates was determined with the corresponding standard deviation. After the analysis of images at very thin areas and in very thick ones, the density of precipitates was determined for each sample. The obtained data were afterwards re-calculated taking the value obtained by Tseng et al. for a sample of the same nominal composition aged at 200 °C for 3 h as a reference (volume fraction 34.3%). This value was used as a reference since it was obtained by using Atom Probe which is a highly precise technique [16]. A correction factor was obtained in this way, which enabled to correct the obtained densities for all the other samples.

3. Results and discussion

In a previous work [21], electrical resistivity measurements were performed in samples with similar thermal treatments conditions. It was shown that martensitic transformation temperatures were difficult to determine from electrical resistivity curves due to the strong effect of the magnetic ordering of the bcc phase and the

Table 1
Name of the studied samples and their corresponding ageing treatments. Samples T10, T20 and T3h are kept 30 min at 1200 °C, water quenched at room temperature and further aged at 200 °C during 10, 20 and 180 min respectively.

Sample	Thermal Treatment
WQ	30 min at 1200 °C and water quenched
T10	200 °C × 10 min
T20	200 °C × 20 min
T3h	200 °C × 3 h

antiferromagnetic ordering of the fcc [22]. In Ref. [21] it was reported that as the ageing time at 200 °C increases, the measured hysteresis in the electric resistivity vs. temperature curve decreases. Such behavior must be ascribed to a reduction in the amount of thermally-induced martensite and is a consequence of a downward shift of the martensitic transformation temperatures related to the formation and growth of coherent precipitates [4,20]. This shift of transformation temperatures, particularly if M_s is considered, can be clearly observed in Fig. 1 where dilatometry results are shown for several samples. It can be noticed in this figure that dilatometry does not allow to detect the magnetic ordering transitions. Fig. 1 shows the effect of ageing treatments on the martensitic transformation temperature leading to the following values: M_s is −6 °C for sample WQ (water quenched) and decreases for aged samples leading to −21 °C and −96 °C for samples T10 and T20, respectively. In the case of T3h, M_s could not be detected after cooling down to liquid nitrogen temperature. This decrease in M_s as the ageing time at 200 °C increases implies a stabilization of the austenite which can be related to the effect of B2 nanoprecipitates on the transformation [4,8]. For the longest ageing time studied (3 h) the martensitic transition has been completely inhibited. Due to this fact, it is particularly interesting to focus the attention on the early stages of precipitation, where the martensitic transition is still clearly detected.

In order to analyze the effect of the thermal treatments on the microstructure, several samples with different thermal treatments were observed by means of TEM. A quantitative analysis of the size and density of precipitates was performed by using the obtained TEM images. As an example, a dark field image corresponding to T3h sample is shown in Fig. 2. Images obtained for samples aged for shorter times at 200 °C can be observed in Ref. [21]. The spot used to obtain this image is identified by an arrow in the corresponding inset of figure. As we reported in Ref. [21], the first noticeable feature is that precipitates are already present in the WQ sample. This finding indicates that precipitates are either introduced during the ageing at 1200 °C or during quenching. In order to assess this aspect, different quenching treatments were performed by either varying the samples thickness or the type of quenching (i.e., directly in water or by placing the sample inside a Fe holder). In all cases, similar precipitates were observed. Comparable results were obtained by Tseng et al. in samples quenched from 1200 °C [8]. No β-Mn precipitates were observed, as it was the reported case of samples where the bcc structure was obtained after quenching with low cooling rates [23].

A systematic analysis involving all samples allowed following the evolution of precipitation after different time intervals at

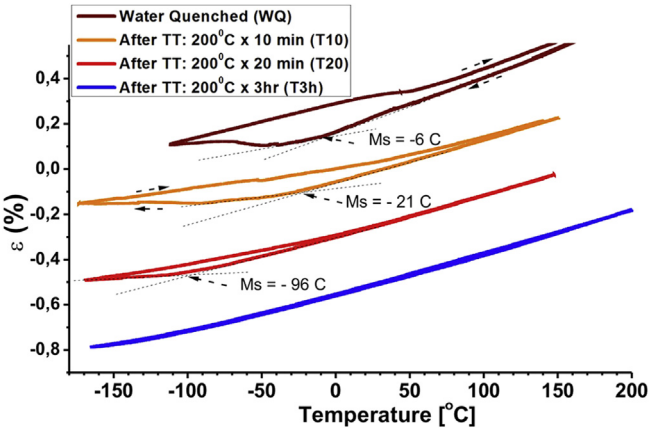

Fig. 1. Dilatometry measurements vs. temperature for alloys WQ, T10, T20 and T3h.

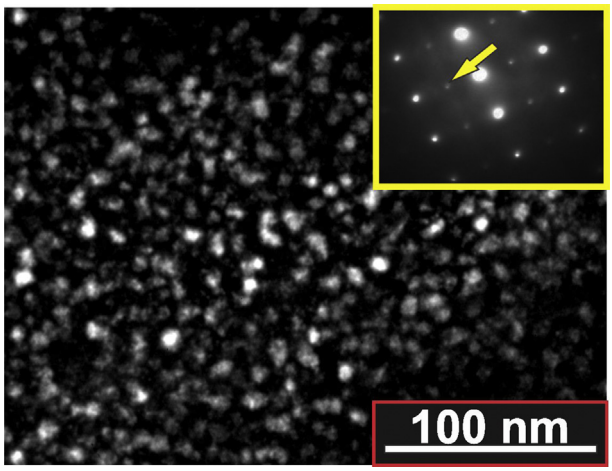

Fig. 2. Dark field TEM image of T3h sample. The diffraction spots used for the images are indicated by arrows in the corresponding inset. Zone axis $[011]_{bcc}$.

200 °C. Additionally, the volume fraction F_v and average distance between particles r has been obtained considering spherical precipitates with diameter d. The obtained F_v data, treated as described in Section 2, and measured M_s values are shown in Table 2.

As ageing at 200 °C proceeds, the average size of precipitates increases and the average distance between precipitates decreases. After 3 h, precipitates are about 50% bigger and 50% closer than those found in the WQ condition. These changes lead to an increased volume fraction which becomes 40 times larger for sample T3h if compared with the initial condition (WQ sample). Recently, similar results were obtained by Tseng et al. [8] by using Atom Probe techniques. Precipitate sizes reported by these authors are slightly smaller than those reported here, although the differences may be explained by uncertainties in the different experimental techniques.

Considering the microstructural parameters described in Table 2, it is clear that a diffusive mechanism takes place during ageing at 200 °C, which affects the B2 precipitates. The microstructural changes related with the nanoprecipitates distribution and size evolution affect the relative phase stability and the thermoelastic character of the stress-induced martensitic transformation [4,8]. In order to achieve a thermoelastic behavior the phase transformation has to meet two requirements. First, the involved structures (austenite and martensite) should have a group-subgroup symmetry relationship, so-called G-subG relation, in order to undergo a martensitic transformation without the need of introducing irreversible changes (such as plastic glide) [24,25]. Second, the volume change between both phases should be small enough to allow the involved deformations to be elastically accommodated. The reported volume change associated to the α-γ′ martensitic transition in Fe-Mn-Al alloys is −0,374% [7] which results in a favorable condition in relation to this second requirement. Considering the first requirement, a high density of precipitates,

Table 2
Measured mean precipitate sizes (d), precipitate volume fractions (F_v), average distance between precipitates (r) and M_s temperatures obtained by dilatometry measurements after different ageing times at 200 °C.

Sample	d [nm]	F_v [%]	r [nm]	M_s [°C]
WQ	8 ± 2	0.78	33	−6 ± 5
T10	8 ± 3	1.06	29	−21 ± 5
T20	9 ± 3	3.64	22	−96 ± 5
T3h	12 ± 2	34.3 (Ref. [8])	15	–

like that determined here after ageing at 200 °C (Table 2) might play a significant role on suppressing irreversible deformation mechanisms. In fact, it has been widely accepted that coherent nanoprecipitates strongly favor hardening in the Fe-Ni-Co system leading to thermoelasticity [3,10,11]. Similar effects of nanoprecipitates were reported for other SMA systems [26].

Fig. 3a shows a TEM micrograph obtained from sample WQ in a region where austenite and martensite phases coexist. The B2 precipitates are present in both phases. The martensitic structure presents several zones with a strong elastic contrast due to the accommodation of precipitates. No distortion is observed around precipitates in the bcc phase but Fig. 3b shows an enlarged view of a martensite zone where the distorted areas extend about 20 nm around precipitates. These observations can be well explained considering results reported by Omori et al. [20]. These authors have shown that in Fe-Mn-Al-Ni alloys, B2 nanoprecipitates are coherent with both structures, austenite and martensite, and that they get sheared during the martensitic transformation. The distortion is elastically accommodated, and the inclination angle is about 4–5° (i.e., the diameter tilt of a precipitate which is considered to be spherical in the parent phase) [20]. Another interesting result is the absence of a well defined habit plane (Fig. 3a), which seems to be a consequence of the lattice distortion around the precipitates. This observation is in agreement with the findings reported in Ref. [20] where the coherence of precipitates and martensite was clearly shown in images obtained by HRTEM. The observed situation is schematically represented in Fig. 3c.

When the martensitic transformation takes place, the elastic energy required for distorting the precipitates and the martensite plays the role of a resistance to the transformation due to the elastic energy barrier that must be overcome to enable the transition. An additional amount of driving force will thus be required for compensating the mentioned resistance to the transformation, an effect that produces a shift of M_s to lower temperatures. If the density and size of precipitates increases by thermal ageing at 200 °C, and provided that they remain coherent, the accumulated elastic energy will also increase when the material undergoes a martensitic transformation. As a consequence, a further decrease of M_s will result from the ageing stage leading, on cooling, to a smaller transformed volume as it was revealed by the dilatometry measurements. Based on these concepts, a model will be presented in order to estimate the energy barrier introduced by the precipitates when they are distorted during the martensitic transformation, and to establish a relationship between the microstructural changes introduced by the thermal treatments at 200 °C and the observed shifts in M_s.

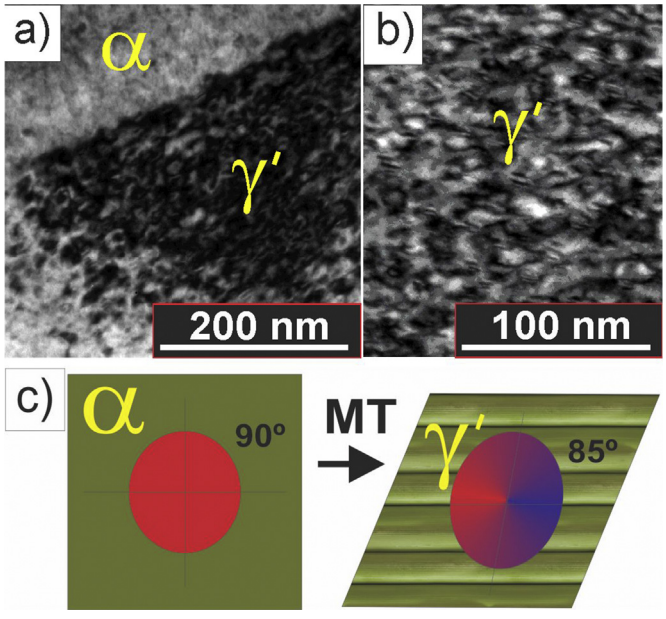

Fig. 3. Transmission electron images obtained for sample WQ: a) Bright field TEM micrograph showing an austenite (α) – martensite (γ′) interface and b)Zoom of a), the martensite phase and coherent precipitates within this phase are elastically distorted. **c)** Schematic distortion of the B2 coherent precipitate when the martensitic transformation takes place.

Eq. (1) shows the energy balance taking place during the α-γ′ transformation:

$$\alpha \rightarrow \gamma' : \quad \left|\Delta G^{\alpha\rightarrow\gamma'}\right| = \Delta G^{res} + E^{p} \tag{1}$$

$\Delta G^{\alpha\rightarrow\gamma'}$ is the value of the required chemical driving force to start the α-γ′ transformation, ΔG^{res} accounts for all inherent contributions to the resistance to the transformation and E^P is the elastic energy contribution added by the presence of coherent precipitates, i.e., it accounts for the elastic distortion energy of precipitates and martensite. E^P will change with the volume fraction of precipitation and, being a stored elastic energy, it will contribute to the retransformation as a back-stress, favoring the thermoelastic character of the transformation.

Considering that the entropy change between austenite and martensite ($\Delta S^{\alpha\rightarrow\gamma'}$) does not significantly change with temperature in the analyzed temperature range, the total Gibbs energy difference can be approximated by $\left|\Delta G^{\alpha\rightarrow\gamma'}\right| = \Delta S^{\alpha\rightarrow\gamma'}(T - T_0)$, where T_0 is the temperature at which the chemical Gibbs energies of the austenite and martensite phases are equal and T the temperature at which the driving force is evaluated [27].

Eq. (1) can now be applied to materials treated during different ageing times, where temperature is selected as the start of the martensitic transformation (M_s). Examples are shown for WQ and T3h samples in Eqs. (2) and (3).

$$\alpha \rightarrow \gamma'(WQ) : \quad \Delta S^{\alpha\rightarrow\gamma'}\left(M_s^{WQ} - T_0\right) = \Delta G^{res} + E^{p}_{WQ} \tag{2}$$

$$\alpha \rightarrow \gamma'(T3h) : \quad \Delta S^{\alpha\rightarrow\gamma'}\left(M_s^{T3h} - T_0\right) = \Delta G^{res} + E^{p}_{T3h} \tag{3}$$

E^{p}_{WC} and E^{p}_{T3h} correspond to the stored elastic energy in samples WQ and after 3 h ageing at 200 °C, respectively. By subtracting Eq. (2) to Eqs. (3) and (4) is obtained. $\Delta S^{\alpha\rightarrow\gamma'}$ can be considered as being independent of temperature based on the linear relationship between the critical stresses to transform from α to γ′ over the analyzed temperature range [4]. According to Omori et al., $\Delta S^{\alpha\rightarrow\gamma'} = -5.84 \times 10^4$ J/m^3 K. Then:

$$\Delta M_s = M_s^{T3h} - M_s^{WC} = \left(E^{p}_{T3h} - E^{p}_{WC}\right) \Big/ \Delta S^{\alpha\rightarrow\gamma'} \tag{4}$$

This equation estimates the shift in M_s temperature, which is required to get an increase of the driving force which is needed to overcome the elastic energy E^p stored due to the presence of nanoprecipitates. The expression is consistent with similar analyses reported in the literature [27–29].

Finally, in order to obtain the shift in M_s, it is required to estimate the contribution of precipitates to the elastic energy (E^p), which will depend on the parameters presented in Table 2. It should be mentioned that two contributions to the elastic energy are to be taken into account: the stored energy in the nanoprecipitates and the energy which is stored in the martensite phase where the precipitates are distributed. However, the second term can be neglected as a first approximation since the martensite can

form nanotwins to relax the stored elastic energy as it has been reported in Ref. [20]. Due to this fact, only the elastic energy per unit volume related to the distortion of the precipitates will be taken into account [20]. We consider an isotropic spherical precipitate which is deformed by a shear strain θ equal to 4° (69.8 mrad) as it was reported in Ref. [20]. The associated elastic energy per unit volume [30] is shown in Eq. (5) and depends on the volume fraction of precipitation F_v.

$$E^p(d,r) = \frac{E}{4(1+\vartheta)}.\theta^2.F_v(d,r) \quad (5)$$

E and υ in Eq. (5) are the elastic modulus and Poisson coefficient, considered as 200 GPa and 0.25, respectively. These values were obtained from the work by Zhang et al. [31]. These authors determined the elastic constants of ordered BCC structures in Fe-Mn-Al alloys, i.e. composition and structure quite similar to that found in the present precipitates [8]. In fact reported results indicate that both elastic constants show values in the ranges ($168 < E < 256$) MPa and $0.236 < \upsilon < 0.265$, depending on the alloy composition [31]. Values of F_v are obtained from Table 2. The experimental and calculated values of ΔM_s for samples used in the present manuscript are shown in Table 3.

As it can be seen from Eq. (5) the increase in F_v, resulting from longer ageing times at 200 °C, leads to an increase on the contribution of precipitates to the elastic energy. It is noticeable the good agreement which can be observed comparing the measured shifts in M_s determined by dilatometry measurements and those obtained by the simplified model which leads to Eq. (4). An interesting point arises if the shift of M_s for sample T3h is considered. The obtained value applying Eq. (5) reaches −1034 °C which has no physical meaning and only indicates that there is no M_s for this condition. Dilatometry measurements are consistent with this finding (Fig. 1). Furthermore, reports where liquid Helium temperature was reached lead to the same result [4,8]. When considering the stress induced martensite, the situation is different. In fact Omori et al. reported a Claussius-Clapeyron relationship where $\frac{\partial\sigma}{\partial T} = 0.53$ Mpa/°C, being σ the critical stress to induce the α-γ′ transformation [4]. Using this value and the obtained shift in M_s for T3h sample (compared to WQ sample), a critical transformation stress of 500 MPa can be estimated for a tensile test at room temperature, which shows a reasonable agreement with values reported for polycrystalline samples in several papers [17,18].

It is noticed that this model quantifies only the precipitate elastic energy contribution to the energy barrier, but other possible factors such as the change in composition of the matrix due to the presence of precipitates might affect the M_s [8]. However, further experiments are necessary to quantify the effect of the later contribution. On the other hand, the presence of an elastic contribution due to the distorted precipitates embedded in martensite is clearly visible (Fig. 3a–b).

There is another relevant point to consider concerning the contribution of the accumulated elastic energy on the M_s shift. The strong effect of nanoprecipitates on M_s is a consequence of the small entropy change between the austenite and martensite structures. In fact, the small magnitude of the entropy change gives rise to two relevant properties of this α-γ′ martensitic transformation: a slight dependence of the critical stress to transform as a function of temperature and a strong effect of any reversible energy contribution on the M_s temperature. Moreover, if the elastic energy contribution is overcome by an applied stress, this energy term will favor the retransformation making it possible to have the pseudoelastic effect. An additional effect of the precipitates on the hardness of the involved structures will also contribute to the pseudoelastic effect decreasing the probability of activating irreversible microstructural mechanisms [8].

Table 3
Measured mean precipitate size (d), precipitate volume fraction (F_v), measured ΔM_s and calculated ΔM_s temperatures obtained by Ec. 4.

Sample	F_v [%]	d [nm]	ΔM_s [°C] exp.	ΔM_s [°C] model
WQ	0.78	8 ± 2	0	0
T10	1.06	8 ± 3	−15	−9
T20	3.64	9 ± 3	−90	−88
T3h	34.3	12 ± 2	–	−1034

4. Conclusions

Several points can be emphasized as conclusions of the present manuscript. The first one concerns the presence of precipitates already in the WQ samples. These precipitates form in austenite keeping a high degree of coherency with this structure. Additional thermal treatments at 200 °C enable diffusive mechanisms which lead to an increase of size and density of precipitates. These values, as well as volume fraction of precipitates, have been determined for several ageing times at 200 °C. The precipitation evolution produces a strong shift of M_s to lower temperatures, leading to a decrease in the amount of thermally-induced martensite and finally to a complete inhibition of the transformation. Observations performed by TEM enabled to detect strong elastic deformation contrast around precipitates in the martensitic structure. The precipitates, although distorted, keep coherency with the martensite. Using the obtained data concerning size of precipitates and volume fraction, the elastic energy contribution of precipitates was estimated by a phenomenological model. This model allows estimating the shift in M_s associated to different ageing times at 200 °C in comparison with the WQ sample. The results indicate that the model can be considered as a good approximation to explain the suppression of the thermally-induced martensitic transition in specimens aged for 3 h at 200 °C, a thermal treatment that enables the alloy to achieve excellent pseudoelastic properties [4,5,8]. In fact the elastic distortion of precipitates once they are in martensite, might play the main role in the retransformation driving force, originating the pseudoelastic behavior.

Acknowledgments

The authors thank financial support from ANPCyT (PICT-2012-0884), CONICET (PIP 112-201001-00056) and UNCUYO (06/C463). E. Aburto and M. Isla helped with quartz capsules.

References

[1] K. Otsuka, C.M. Wayman (Eds.), Shape Memory Materials, Cambridge University Press, 1998.
[2] T. Toneyama, S. Miyazaki (Eds.), Shape Memory Alloys for Biomedical Applications, CRC Press, 2009.
[3] Y. Tanaka, Y. Himuro, R. Kainuma, Y. Sutou, T. Omori, K. Ishida, Ferrous polycrystalline shape-memory alloy showing huge superelasticity, Science 327 (2010) 1488–1490.
[4] T. Omori, K. Ando, M. Okano, X. Xu, Y. Tanaka, I. Ohnuma, R. Kainuma, K. Ishida, Superelastic effect in polycrystalline ferrous alloys, Science 333 (2011) 68–71.
[5] T. Omori, M. Okano, R. Kainuma, Effect of grain size on superelasticity in Fe-Mn-Al-Ni shape memory alloy wire, Appl. Mater. 1 (2013) art. 032103.
[6] P. Krooss, C. Somsen, T. Niendorf, M. Schaper, I. Karaman, Yu.I. Chumlyakov, G. Eggeler, H.J. Maier, Cyclic degradation mechanisms in aged FeNiCoAlTa shape memory single crystals, Acta Mater. 79 (2014) 126–137.
[7] K. Ando, T. Omori, I. Ohnuma, R. Kainuma, K. Ishida, Ferromagnetic to weak-magnetic transition accompanied by bcc to fcc transformation in Fe–Mn–Al alloy, Appl. Phys. Lett. 95 (2009) art. 212504.
[8] L.W. Tseng, Ji. Ma, B.C. Hornbuckle, I. Karaman, G.B. Thompson, Z.P. Luo, Y.I. Chumlyakov, The effect of precipitates on the superelastic response of [100] oriented FeMnAlNi single crystals under compression, Acta Mater. 97

(2015) 234–244.
[9] I.V. Kireeva, Yu.I. Chumlyakov, V.A. Kirillov, I.V. Kretinina, Y.N. Danil'son, I. Karaman, E. Cesari, Thermoelastic γ–α′-martensitic transformations in FeNiCoAlTa aging single crystals, Russ. Phys. J. 53 (2011) 1103–1106.
[10] J. Ma, B.C. Hornbuckle, I. Karaman, G.B. Thompson, Z.P. Luo, Yu.I. Chumlyakov, The effect of nanoprecipitates on the superelastic properties of FeNiCoAlTa shape memory alloy single crystals, Acta Mater. 61 (2013) 3445–3455.
[11] Y. Geng, D. Lee, X. Xu, M. Nagasako, M. Jin, X. Jin, T. Omori, R. Kainuma, Coherency of ordered γ′ precipitates and thermoelastic martensitic transformation in FeNiCoAlTaB alloys, J. Alloy. Compd. 628 (2015) 287–292.
[12] J. Mino, V. Komanicky, M. Durisin, K. Saksl, J. Kovac, R. Varga, Structural and magnetic characterization of Fe-Mn-Al-Ni Pseudo-Heusler alloy, IEEE Trans. Magn. 51 (2015) art. 4000903.
[13] L.W. Tseng, Ji Ma, M. Vollmer, P. Krooß, T. Niendorf, I. Karaman, Effect of grain size on the superelastic response of a FeMnAlNi polycrystalline shape memory alloy, Scr. Mater. 125 (2016) 68–72.
[14] T. Omori, H. Iwazako, R. Kainuma, The abnormal grain growth induced by cyclic heat treatment in Fe-Mn-Al-Ni superelastic alloy, Mater. Des. 101 (2016) 263–269.
[15] L.W. Tseng, Ji. Ma, S.J. Wang, I. Karaman, M. Kaya, Z.P. Luo, Y.I. Chumlyakov, Superelastic response of a single crystalline FeMnAlNi shape memory alloy under tension and compression, Acta Mater. 89 (2015) 374–383.
[16] L.W. Tseng, Ji. Ma, S.J. Wang, I. Karaman, Yu.I. Chumlyakov, Effects of crystallographic orientation on the superelastic response of FeMnAlNi single crystals, Scr. Mater. 116 (2016) 147–151.
[17] M. Vollmer, C. Segel, P. Krooss, J. Günther, L.W. Tseng, I. Karaman, A. Weidner, H. Biermann, T. Niendorf, On the effect of gamma phase formation on the pseudoelastic performance of polycrystalline Fe-Mn-Al-Ni shape memory alloys, Scr. Mater. 108 (2015) 23–26.
[18] M. Vollmer, P. Krooss, M.J. Kriegel, V. Klemm, C. Somsen, H. Ozcan, I. Karaman, A. Weidner, D. Rafaja, H. Biermann, T. Niendorf, Cyclic degradation in bamboo-like Fe-Mn-Al-Ni shape memory alloys- the role of grain orientation, Scr. Mater. 114 (2016) 156–160.
[19] T. Niendorf, F. Brenne, P. Krooss, M. Vollmer, J. Günther, D. Schwarze, H. Biermann, Microstructural evolution and functional properties of Fe-Mn-Al-Ni ahape memory alloy processed by selective laser melting, Metall. Mater Trans. A (2016) 2569–2573.
[20] T. Omori, M. Nagasako, M. Okano, K. Endo, R. Kainuma, Microstructure and martensitic transformation in the Fe-Mn-Al-Ni shape memory alloy with B2-type coherent fine particles, Appl. Phys. Lett. 101 (2012) art. 231907.
[21] P. La Roca, J. Medina, C.E. Sobrero, M. Avalos, J.A. Malarria, A. Baruj, M. Sade, Effects of B2 nanoprecipitates on the phase stability and pseudoelastic behavior of Fe-Mn-Al-Ni shape memory alloys, in: MATEC Web of Conferences 33, 2015, p. 04005.
[22] Y.S. Zhang, X. Lu, X. Tian, Z. Qin, Compositional dependence of Néel transition, structural stability, magnetic properties and electrical resistivity in Fe-Mn-Al-Cr-Si alloys, Mater Sci. Eng. A 334 (2002) 19–27.
[23] P. Huang, H. Peng, S. Wang, T. Zhou, Y. Wen, Relationship between martensitic reversibility and different nano-phases in FeMnAlNi shape memory alloys, Mater Char 118 (2016) 22–28.
[24] K. Bhattacharya, S. Conti, G. Zanzotto, J. Zimmer, Crystal symmetry and the reversibility of martensitic transformations, Nature 428 (2004) 55–59.
[25] K. Otsuka, A. Saxena, J. Deng, X. Ren, Crystal symmetry and the reversibility of martensitic transformations, Philos. Mag. 91 (2011) 4514–4535.
[26] F.d.C. Bubani, M. Sade, F. Lovey, Improvements in the mechanical properties of the 18R ↔ 6R high-hysteresis martensitic transformation by nanoprecipitates in CuZnAl alloys, Mat. Sci. Eng. A 543 (2012) 88–95.
[27] J.R.C. Guimarães, Excess driving force to initiate martensite transformation in fine-grained austenite, Scr. Mater. 57 (2007) 237–239.
[28] L. Kaufman, M. Cohen, Thermodynamics and kinetics of martensitic transformations, Prog. Metal. Phys. 7 (1958) 165–246.
[29] P. La Roca, L. Isola, Ph. Vermaut, J. Malarria, Relationship between martensitic plate size and austenitic grain size in martensitic transformations, Appl. Phys. Lett. 106 (2015) art. 221903.
[30] J.F. Nye, Physical Properties of Crystals: Their Representation by Tensors and Matrices, Clarendon Press - Oxford, New York, United State, 1998.
[31] H. Zhang, S. Lu, M. Zhou, M.P.J. Punkkinen, B. Johansson, L. Vitos, Ab initio determination of the elastic properties of ferromagnetic body-centered cubic Fe-Mn-Al alloys, J. Appl. Phys. 118 (2015) art. 103904.